Design and Optimization of Linear Synchronous Motors for Transportation Applications

Soheil Fattahpour Roushan[1], Abbas Shiri[2,*], and Peyman Naderi[3]

[1]Faculty of Electrical Engineering, Shahid Rajaee Teacher Training University, Tehran, Iran, s.fattahpour@sru.ac.ir,

[2,*] Corresponding author: Faculty of Electrical Engineering, Shahid Rajaee Teacher Training University, Tehran, Iran, abbas.shiri@sru.ac.ir, phone: +98-21-22970053 (2460), ORCID: 0000-0001-5672-0670

[3]Faculty of Electrical Engineering, Shahid Rajaee Teacher Training University, Tehran, Iran, p.naderi@sru.ac.ir,

Abstract

This paper presents a method for designing single-sided linear synchronous motor (SSLSM). In the proposed method, electrical circuit equations of the linear synchronous motor (LSM) at steady-state are used. In addition, a new method is proposed to model the "end effect" phenomenon by deriving an effective field current. To do this, induced currents in rail-way windings due to DC-excitation and the effect of these currents on induced voltage in rail-way windings are considered. So, in addition to the proposed design method, the main contribution of the manuscript is the modeling of the end effect in LSMs. Due to its simplicity, the proposed design method can be easily used in optimization of LSM that requires iterative algorithms. Therefore, by choosing appropriate design variables, an optimization is done to maximize efficiency and power factor of the motor as well as to minimize mover and rail weights. To validate the optimized design, 3-D Finite Element Method (FEM) is used. The comparison of the results of the FEM and the proposed method confirms the accuracy and effectiveness of the latter.

Keywords— Linear synchronous motor, End effect, DC-Excited, Design Optimization, Finite Element Method.

1. Introduction

Recently, many industry apparatuses have been driven by linear motors. By eliminating gears and mechanical intermediates, linear motors can be used to drive a linear motion load. Among linear motors, linear synchronous motors (LSMs) have been used for transportation applications due to their manifest advantages [1]-[3]. LSMs usually have higher values of power factor and efficiency in comparison with the linear induction motors (LIMs). By proper control, the input power factor can experience higher values than the power factor of a comparable LIM, at the same speed and output power. In addition, substantial cost saving is a result of inverter rating reduction due to higher values for power factor and efficiency [4], [5].

In works in the literature, many features of LSMs, including analysis, modeling, design and control have been discussed [6]-[14]. In [6], the operating principle of the LSM has been discussed and the effect of the entry and exit end effect on the thrust and power loss has been investigated. A 2-D analytical model for flat linear permanent-magnet has been proposed in [7]. Some researchers have concentrated on thrust ripple mitigation [8]-[10]. Most of them have focused on rearrangement of permanent magnets. To investigate the performance and calculate the forces of the LSMs, many researchers have employed FEM [11]-[15]. This method is usually time-consuming and is not suitable for optimization. The techniques used for modeling and design of LSMs in most researches are mathematically complicated [16]-[21]. In [16], Neural Network and FEM have been employed to improve the efficiency of the permanent magnet LSM (PMLSM). The design and analysis have been done on the basis of 2-D analytical field analysis in [17]. In [18], the guidance force has been calculated by conformal mapping method. Also, cogging force has been minimized by using FEM in [19]. In [20], the design of PMLSM with trapezoidal permanent magnets has been optimized. Electromagnetic analysis has been used to model the motor. In other researches, magnetic equivalent circuit has been employed for design, modelling and fault diagnosis [22]-[24]. There are many analytical works in literature on optimization of linear induction motors which have used circuit model methods for designing [25]-[27]. These methods simplify the sensitivity analysis and optimization. However, the modelling and design of the LSMs have been done by using numerical and electromagnetic methods. Therefore, these methods add computational burden to the design process. In addition, the end effect phenomenon has not been quantitatively presented in literature for LSMs.

In [28], a simple method for the design of DC excited linear synchronous motor (DCELSM) has been proposed. In this paper, the method presented in [28] is modified and completed. Modeling the end effect phenomenon and including it in design is one of the contributions of the current paper. In addition, the other contribution of the

paper is to present a design method which is more suitable for optimization purposes due to reducing the design complexity. In the following, the motor structure is discussed in section 2; the modeling and performance calculations are done in section 3; following, the end-effect calculations are presented and discussed. The procedure of the design is introduced in section 4. In sections 5 and 6, the optimization method as well as its results are given and discussed. Finally, the results obtained by the proposed optimization method are validated by 3-D FEM, following by the conclusion remarks.

2. Motor Structure

A schematic of a single-sided wound mover linear synchronous motor (WMLSM) with a long stator is illustrated in Fig. 1. As it is seen in the figure, the stator of the motor which is extended along the rail-way includes 3-phase iron-cored windings. The copper windings laid into the open slots which are developed through the stator iron core. The stator (rail-way) is divided into two parts, energized and non-energized sections. The length of the rail (stator) which is chosen to be energized is about five times of the mover length (see Fig. 1). The moving part is located above the stator consists of the iron core and the DC-excited field.

Fig. 1 Approximately here

3. Performance Calculations

For designing the DCELSMs, the steady-state equations of the motor have been employed. Thus, in the following, the machine steady-state equations are derived.

A. Steady-state equations

Fig. 2 shows the phasor diagram of a linear salient pole synchronous motor in under-excited condition. By using this phasor diagram, the stator input voltage is written as:

$$\overrightarrow{V_1} = R_1\overrightarrow{I_a} + jX_{sd}\overrightarrow{I_{ad}} + jX_{sq}\overrightarrow{I_{aq}} + \overrightarrow{E_f} \tag{1}$$

The d and q-axis components can be separated; so, they are derived as follows:

$$\begin{cases} V_1 \sin\delta = -R_1 I_{ad} + X_{sq} I_{aq} \\ V_1 \cos\delta = R_1 I_{aq} + X_{sd} I_{ad} + E_f \end{cases} \tag{2}$$

Fig. 2. Approximately here

In equations (1) and (2), I_a is the armature current, I_{ad} and I_{aq} are the d and q-axis components of armature current, respectively, E_f is the stator's phase induced voltage due to DC excitation and δ is the load angle. The parameters, R_1, X_{sd} and X_{sq} are resistance of the armature, reactances of d and q-axis, respectively which are given as follows [1], [5]:

$$R_1 = \rho_w \frac{l_w}{A_w} \tag{3}$$

$$\begin{cases} X_{sd} = X_1 + X_a + X_{ad} \\ X_{sq} = X_1 + X_a + X_{aq} \end{cases} \tag{4}$$

where ρ_w is the stator windings' electrical resistivity, l_w is the length of the stator windings and A_w is the conductor's cross-section. Also, X_1, X_a, X_{ad} and X_{aq} respectively are leakage reactance of the armature under the mover, armature reactance due to the magnetic flux paths in the air with no exciter underneath, d and q-axis reaction reactances of the armature which are calculated as follows [1], [5]:

$$X_1 = 2\mu_0\omega_1[(\lambda_s + (\frac{N_1}{N_2})\lambda_d)l + \lambda_e l_{ec}](\frac{N_1 N_2}{pq}) \tag{5}$$

$$X_a = \frac{2\mu_0\omega_1 l(N_2 - N_1)}{\pi} \tag{6}$$

$$X_{ad} = \frac{2\mu_0\omega_1\tau l N_1^{\,2}}{\pi^2 k_c g_0 p} k_{ad} \tag{7}$$

$$X_{aq} = \frac{k_{aq}}{k_{ad}} X_{ad} \tag{8}$$

In the above equations, μ_0 is the vacuum (or air) permeability, ω_1 is input angular frequency, λ_s, λ_d and λ_e are specific permeances of slot, differential and end-connection, respectively, N_1 and N_2 are the series turns per phase number under mover and at the empty stator energized section, respectively, l the armature stack width, l_{ec} length of the end-connection, p the pole pairs, q the slots per pole per phase, τ the pole pitch, k_c the Carter's coefficient, g_0 the length of the air-gap, X_{ad} and X_{aq} are the form factors of the d and q-axis of the armature reaction, respectively which are derived by the following equations:

$$\begin{cases} k_{ad} = [\pi\alpha_p + \sin(\pi\alpha_p)]/\pi \\ k_{aq} = [\pi\alpha_p - \sin(\pi\alpha_p)]/\pi \end{cases} \quad (9)$$

Where α_p is the ratio of the pole arc. Also, in (1), E_f can be written as:

$$E_f = \sqrt{2} B_f \, lN_1 u_s \quad (10)$$

in which, u_s is the synchronous speed and B_f is the air-gap flux density due to DC excitation. These parameters are calculated by (11) and (12).

$$u_s = 2 f_1 \tau \quad (11)$$

$$B_f = \frac{\mu_0 w_f I_f}{g_0 k_c (1 + k_{sat})} \quad (12)$$

where f_1 is the stator supply frequency, w_f is the number of series turns per pole and k_{sat} is the saturation factor. In the mover circuit, the DC excitation current is calculated as follows:

$$I_f = \frac{V_{dc}}{R_f} \quad (13)$$

in which, V_{dc} is the mover input DC voltage and R_f is its winding resistance which is calculated as follows:

$$R_f = \frac{\rho_{wf} l_{wf}}{A_{wf}} \quad (14)$$

where ρ_{wf} is the DC-excitation windings' resistivity, l_{wf} is the length of the mover windings and A_{wf} is the conductor's cross-section. Now, the primary tooth flux density can be calculated as:

$$B_t = \frac{\tau_s}{w_t} B_1 \quad (15)$$

where w_t is the tooth width and τ_s is slot pitch of the stator. Also, B_1 is the fundamental component of the flux density of the air-gap which can be calculated as follows:

$$B_1 = \frac{E_i}{\sqrt{2}\, lN_1 u_s} \quad (16)$$

where E_i is the total induced voltage RMS value on each stator's phase which can be defined as shown in Fig. 2.

B. End-effect calculations

In the linear induction motors (LIMs), as primary moves, the air-gap flux in the secondary increases and decreases at entry and exit ends of the motor, respectively. Accordingly, it induces currents on the secondary sheet of the motor. So, the secondary sheet can be assumed as different short circuited electrical circuits. The reaction of these short circuits causes the "end effect phenomenon". Total air-gap flux due to the entry and exit end effects exponentially increases along the normalized time (normalized length of the motor) [29]. Also, the induced eddy current in the secondary sheet is in its maximum value at the entry of the motor and then exponentially decreases to zero along with the length of the motor. The normalized length of the motor, Q is calculated as follows [29]:

$$Q = \frac{L_s R_2 \omega_1}{(X_m + X_2)u} \tag{17}$$

In the above equation, L_s is the primary length, R_2 is the secondary resistance, X_m and X_2 are the magnetizing reactance and the secondary leakage reactance, respectively and u is the primary speed in LIMs.

As mentioned above, the induced eddy current in the secondary sheet has exponential form as [29]:

$$I_{2ea} = -I_m e^{-x} \tag{18}$$

So, the average value of the eddy current per unit length is calculated as follows:

$$I_{2e} = -\frac{I_m}{Q}\int_0^Q e^{-x}dx = -(\frac{1-e^{-Q}}{Q})I_m \tag{19}$$

In the above equation, I_m is the magnetizing current which produces the flux.

In the linear synchronous motors (LSMs), the stator windings take the role of the secondary sheet in LIMs. The only difference is that in LSMs, the stator windings are not short circuited but connected to a definite resistance; so, with moving the mover, the changes of the air-gap flux at the entry and exit ends of the machine induces currents in stator windings, causing similar process occurs in LIM.

By using Duncan's model discussed above which has been presented for linear induction motor (LIM) and knowing that there are three phase on rail, the average value of the induced current per unit length of the machine in each phase can be separately calculated as:

$$I_{ia} = -(\frac{1-e^{-Q}}{Q})\frac{I_f}{3} \tag{20}$$

where Q can be calculated as the same manner discussed in [29]. By modifying the Duncan's equation for Q (eq. 17) and considering the stator winding resistance in which the eddy currents flow, the following is derived for LSMs:

$$Q = \frac{L_s R_1 \omega_1}{(X_1 + X_a + X_{ad})u_s} \tag{21}$$

It is clear that the induced currents can cause an extra power loss as it passes through the rail-way windings. Similar to Duncan's method, the power loss due to induced currents is calculated as follows:

$$P_e = (\frac{1-e^{-Q}}{Q})(\frac{I_f}{3})^2 R_{1f} \tag{22}$$

where R_{1f} is the rail-way resistance transferred to the mover part. Now, by replacing R_{1f} in terms of R_1, the whole power loss due to induced currents for all 3-phase coils is calculated as:

$$P_t = \frac{2}{3}(\frac{1-e^{-Q}}{Q})(\frac{I_f}{3})^2(\frac{N_f}{N_1})^2 R_1 \tag{23}$$

In the above equation, N_f is the turn number of field winding and N_1 is the primary winding per-phase turn number. Now, the effect of power loss due to eddy currents is defined by a virtual resistance in the field circuit (see Fig. 3). In this figure, R_{fe} is the virtual resistance representing the power loss due to the end effect (P_t) and I_{fm} is the modified DC-excitation current. It should be remembered that the field current before considering the end effect is I_f. In Fig. 3, the input power is equal to the power losses in resistances R_f and R_{fe}. So, by writing the equation of the power and solving it, the modified DC-excitation current can be derived as:

$$I_{fm} = \frac{V_{dc} + \sqrt{{V_{dc}}^2 - 4R_f P_t}}{R_f} \tag{24}$$

Then, the effective DC-excitation current which passes through the magnetizing branch can be calculated as:

$$I_{fe} = (1 - \frac{1 - e^{-Q}}{Q}) I_{fm} \tag{25}$$

In Fig. 4, the variation of the air-gap flux density versus the motor speed is illustrated. As it is seen in this figure, the air-gap flux density decreases as the motor speed increases. This is because of the reaction of the rail-way windings which increases at high speeds.

Fig. 3 Approximately here

Fig. 4 Approximately here

C. Calculation of the Efficiency and electromagnetic thrust

By ignoring the core loss of the armature, the electromagnetic power is derived as [1]:

$$P_{elm} = 3V_1 I_a \cos\phi - 3R_1 {I_a}^2 \tag{26}$$

where $\cos\phi$ is the stator input power factor (refer to Fig. 2) and I_a is the armature current. Thus, the thrust produced by the machine is calculated as [1]:

$$F_x = \frac{P_{elm}}{u_s} \tag{27}$$

The load-angle (δ) is the other important parameter in LSM. By employing (2) and (26) in (27), the thrust as a function of δ is derived as follows:

$$F_x = \frac{m[V_1(R_1\cos\delta + X_{sd}\sin\delta) - E_f R_1]}{u_s(X_{sd}X_{sq} + {R_1}^2)^2}[V_1(X_{sq}\cos\delta - R_1\sin\delta)(X_{sd} - X_{sq}) + E_1(X_{sd}X_{sq} + {R_1}^2) - E_1 X_{sq}(X_{sd} - X_{sq})] \tag{28}$$

The thrust versus load angle is illustrated in Fig. 5 for a machine with zero and non-zero armature winding resistance. The efficiency can be calculated as follows:

$$\eta = \frac{P_{out}}{P_{in}} = \frac{F_{xo}u_s}{mV_1 I_a \cos\phi} \tag{29}$$

In the above equation, m is the number of the phases and F_{xo} is the output thrust.

D. Weight

The LSM can be divided into the two parts: the rail-way and the mover. The two parts' weights should be calculated, separately. For calculation of the rail-way weight in energized section, the weight of the windings as

well as the core should be calculated. The whole weight of the rail-way in energized section is calculated as follows [28]:

$$W_{1tot} = (m\frac{N_2}{N_1} l_w) A_w \rho_{cu} + [L_s l h_{y1} + N_t l w_t h_s] \rho_{Fe} \quad (30)$$

In the above equation, ρ_{cu} the copper specific weight, h_{y1} the yoke height, N_t the teeth number through the rail-way and ρ_{Fe} is the iron specific weight.

The mover weight is calculated in a similar way accomplished for the stator. The total weight of the machine can be obtained by summing the rail-way and the mover weight.

Fig. 5 Approximately here

4. Design

In this section, a new method is presented in order to design an LSM with desired characteristics such as speed and thrust. The method employs the equations of the motor which have been presented in section 3. The end effect phenomenon has been modeled and taken into account in the design.

A. Stator design

By having the speed and the input frequency, the pole pitch of the LSM is calculated from (11). Then, the length of the mover is calculated by the following equation:

$$L_s = 2p\tau \quad (31)$$

In order to design an effective rail-way, the energized section length should be appropriately chosen. The length of the energized section on the rail-way is calculated as follows:

$$L_{en} = k_{en} L_s \quad (32)$$

where coefficient k_{en} is an proper integer. Choosing low values for k_{en} makes rail-way unfavorable; on the other hand, high values of k_{en} leads to increased resistance of the stator. By calculating the pole pitch and choosing an appropriate value for q (slots/pole/phase), the slot pitch is calculated as:

$$\tau_s = \frac{\tau}{mq} \quad (33)$$

It is necessary to note that the higher values of q reduce the spatial harmonics and the slot width. The slot width reduction is limited by construction considerations. To calculate slot's dimensions, the tooth width is considered as a factor of slot pitch as follows:

$$w_t = c_t \tau_s \tag{34}$$

where c_t is a coefficient which is chosen in [0,1] range. By determining w_t, the slot width is calculated by:

$$w_s = \tau_s - w_t \tag{35}$$

To calculate N_1 and N_2, the number of turns per coil (n_c) and pole pairs are needed. After choosing coil type, at first $n_c = 1$ is chosen and the design is proceeded with this n_c. If the thrust requirements in the design is met, the design is stopped, else n_c is replaced by $n_c + 1$ and the design procedure is repeated. Thus, by having n_c and the coil type, N_1 is calculated as:

$$N_1 = \begin{cases} n_c pq & , \quad one\,layer\,winding \\ 2n_c pq & , \quad two\,layer\,winding \end{cases} \tag{36}$$

N_2 is calculated as:

$$N_2 = k_{en} N_1 \tag{37}$$

where coefficient k_{en} is defined before.

To calculate the other parameters, the stator input current should be estimated. By using equation (29), the estimated stator current is calculated as follows:

$$I_a = \frac{F_{xd} u_s}{m V_1 \eta \cos\phi} \tag{38}$$

where F_{xd} is the desired thrust. To calculate the current, one should choose $\eta \cos\phi$. At the beginning, $\eta \cos\phi$ is chosen in [0,1] range and during the design process, its real value can be calculated. After calculating the electrical parameters and obtaining the actual motor current, these values will be corrected. Now, by estimating the initial current and choosing the current density (j_c) for the primary coil, the slot cross-section area can be calculated as:

$$A_s = \frac{n_c I_a}{k_{fill}\, j_c} \tag{39}$$

in which k_{fill} is slot fill factor. The slot height can be calculated by specifying the slot width and cross-section area as:

$$h_s = \frac{A_s}{w_s} \tag{40}$$

Considering the appropriate coefficient for the electrical equations presented in the preceding section, the electrical parameters of the motor can be calculated. By calculating these parameters and employing equations (1), (2) and the phasor diagram illustrated in Fig. 2, the actual input current can be calculated. It should be noted that the appropriate load-angle can be calculated from the load-angle characteristic of equation (28). To calculate E_f in the above equations, first, a value for the stator tooth flux density is chosen using B-H curve of the iron which is used in the stator structure. Initially, by neglecting the armature reaction effect on the air-gap flux density, an upper bound for the air-gap flux density due to mover DC excitation can be obtained. By choosing an appropriate value for this flux density, induced voltage E_f can be calculated. It should be noted that this choice is appropriate because the motor main flux density is the same as that produced by DC excitation and the changes in the stator electrical parameters will not change it significantly. However, at the end, the real value of the air-gap flux density is calculated by taking into account the armature reaction effect and consequently the actual flux density of the stator tooth can be obtained. When the actual input current of the motor is determined, the power factor and the efficiency can be calculated by using equations (1), (2) and (29) and the phasor diagram shown in Fig. 2. The calculated value for the multiplication of these two can be obtained. If this calculated value is acceptable, the calculation is stopped, if not, a new value is determined by the following equation and the calculation is repeated until the estimated value is converged to the calculated value:

$$(\eta\cos\phi)_{new} = \frac{(\eta\cos\phi)_{cal} + (\eta\cos\phi)_{es}}{2} \tag{41}$$

Now, the thrust can be calculated; if it is close enough to the desired value, we stop the calculations and if not, n_c is replaced by $n_c + 1$ and the calculation is repeated until the thrust error to be acceptable. After all, by determining the number of turns in each coil, the number of series turns in each phase, the corresponding input current and the cross-section area obtained for the conductors, a conductor from standard wire table is selected. Given the selected conductor diameter, the width of the tooth and slot should be recalculated. Now, the flux density in the teeth is calculated from equation (15) and compared with the maximum allowed value. If the flux density is higher than a maximum value, the tooth width should be increased. Finally, the output parameters and the weight of the machine recalculated. Flowchart of the LSM's stator design procedure is illustrated in Fig. 6.

B. Rotor design

By having the air-gap flux density due to DC excitation and using equation (12), the required MMF ($w_f I_f$) can be calculated. By having the MMF, the other parameters can be obtained from equations (13) and (14). To consider the end effect, the effective DC-excitation current is calculated using equations (20) – (25). Then, the flux density as well as the other stator design parameters should be updated by replacing I_f by the calculated effective DC-excitation current in (12).

Fig. 6 Approximately here

5. Optimization

The evolutionary algorithms such as genetic [26], [27], particle swarm optimization [20], [30] etc. have been widely employed in optimization of linear machines. In this paper, the PSO algorithm is used for optimization. In this algorithm, vectors of position and velocity are assigned to each particle. Moreover, each particle has a memory that records its previous best position. Also, all particles record the global best position that a swarm has achieved in their memory. The position and velocity of each particle is updated in each repetition by using the following equation [31]:

$$\begin{aligned} X_i(t) &= X_i(t-1) + V_i(t) \\ V_i(t) &= \omega V_i(t-1) + C_1 r_1 (p_{best_i}(t) - X_i(t-1)) + C_2 r_2 (g_{best}(t) - X_i(t-1)) \end{aligned} \tag{42}$$

where $X_i(t)$ and $V_i(t)$ define the updated position and velocity of i^{th} particle in the search space, respectively, $X_i(t-1)$ and $V_i(t-1)$ are the previous position and velocity of the i^{th} particle, respectively. Also, $p_{best_i}(t)$ and $g_{best}(t)$ are the best personal position of each particle and the best position of all particles, respectively, r_1 and r_2 are two random numbers in the range of [0 1], C_1 and C_2 are learning coefficients and ω is the inertia coefficient. This coefficient can be decreased in order to confine the search space. Proper results can be obtained by using linearly decreasing inertia coefficient [31]. Inertia should be changed from $\omega_{\max}$ to $\omega_{\min}$. It can be expressed as:

$$\omega = \omega_{\max} - \frac{\omega_{\max} - \omega_{\min}}{iter_{\max}} \times iter \tag{43}$$

In (43), $iter$ and $iter_{\max}$ respectively are the iteration number and the final iteration number. The procedure of the PSO is illustrated in Fig. 7. The procedure implementing the PSO algorithm can be found in [31].

Fig. 7 Approximately here

6. Optimization Results

In this section, at first, the method presented in section 4 is used to design a motor and then the PSO algorithm presented in section 5 is employed to optimize the design. MATLAB software is used for design and optimization. The motor is designed to have (1000 ± 50)N output thrust in synchronous speed of $u_s = 5m/s$. Other specifications that are used for optimization are given in Table I. The cost functions are defined as power factor, efficiency, mover weight and rail-way weight per meter. In first scenario, the cost functions have been optimized, separately; the results are shown in Table II. As it is seen in the table, the power factor and the efficiency have been obtained 1 and 76%, respectively. Also, the weight of the rail per meter and the mover weight have been obtained 61.1 kg and 71.2 kg, respectively.

In the second scenario, all of outputs have been optimized simultaneously as a multi-objective function. The results are shown in Table III and IV. To optimize all objective functions together, they have been defined as a single function as below:

$$M = fu_1 \times fu_2 \times fu_3 \tag{44}$$

where fu_1 and fu_2 are the objective functions referred to the power factor and efficiency, respectively and fu_3 is the objective function referred to the machine weight which is expressed as:

$$fu_3 = \frac{(\frac{1}{W_{metr}} + \frac{1}{W_{tp2}})}{2} \tag{45}$$

where W_{metr} and W_{tp2} are the rail-way weight per meter and the mover weight, respectively. As it is seen in Table IV, the power factor is 0.904 and the efficiency is 63.36 which both are lower than those of obtained in single-optimization scenario.

For optimization in this paper, ω has linearly changed from 1.5 to 0.5, C_1 and C_2 are 2 and 1.5, respectively. Also, the population number is 900. The maximum number of iteration is 500.

Table I Approximately here

Table II Approximately here

Table III Approximately here

Table IV Approximately here

7. Validation

2-D and 3-D FEM have been employed to validate the optimized motor results with parameters illustrated in Table III. The Ansoft/Maxwell has been used to simulate the optimized motor. In simulations, 3-phase voltage source has been applied to the rail-way. To shorten the simulations transient time, the initial speed of the motor has been set to 5 m/s. The mover circuit has been supplied with constant DC current. The flux density distribution and the flux lines in different parts of the motor are shown in Figs. 8 and 9, respectively. It is seen in Fig. 8 that the maximum flux density is about 2T which occurs in the mover yoke. The 3-D configuration of the motor in Asoft/Maxwell environment is illustrated in Fig. 10. Fig. 11 illustrates the thrust of the motor at full-load. There are some ripples in the output thrust, however, its average value is equal to 953.4N. Fig. 12 also shows the input 3-phase currents at full-load. The currents peak values are 18.4 A.

To make fair comparison, the proposed method results at 2 loads (full-load and about half-load) have been compared with the results of the 2-D and 3-D FEM in Table V. Comparing the results show that there is an acceptable accordance between the results of the FEM analysis and those of obtained by the proposed method. For example, at full-load, the highest error between proposed method and the 3-D FEM is related to the efficiency which is 3.3%. As it is seen in the table, the efficiencies obtained by 3-D FEM at both loads are lower than those of obtained by the proposed method. This is because of the inclusion of the core loss in the FEM calculations, while it is not considered in the proposed method.

Fig. 8 Approximately here

Fig. 9 Approximately here

Fig. 10 Approximately here

Fig. 11 Approximately here

Fig. 12 Approximately here

Table V Approximately here

8. Conclusion

An effective design method has been presented to design DC-excited LSM. In addition to its simplicity, the proposed method has ability in optimization and sensitivity analysis. In contrary, in the numerical methods due to their high calculation burden, these tasks are very difficult. The end effect phenomenon has been modeled as field current drop and considered in the design equations. The sensitivity analysis has been done by using the proposed

method. The single and multi-objective optimization methods based on PSO algorithm have been performed to optimize the power factor, efficiency and the weight of the primary/meter and the mover. The results of the optimized motor have been compared with the results of 2-D and 3-D finite element analysis. The comparison shows a good agreement between two methods' results, confirming the accuracy of the proposed design method and optimization.

Acknowledgement

This work was supported by Shahid Rajaee Teacher Training University under Grant Number of 5973/82.

9. References

[1] Gieras J. F., Piech Z. J., and Tomczuk B., "*Linear synchronous motors: transportation and automation systems",* CRC press (2018), doi: 10.1201/b11105.

[2] Krämer C., "Magnetic Equivalent Circuit Modeling and Optimal Control of a Permanent Magnet Linear Synchronous Motor*", Shaker Verlag GmbH Press*, (2023), doi: http://hdl.handle.net/20.500.12708/175839.

[3] Krämer C., Kugi A., Kemmetmüller W., "Modeling of a permanent magnet linear synchronous motor using magnetic equivalent circuits", *Mechatronics*, **76**(9), pp. 1-9 (2021) doi: 10.1016/j.mechatronics.2021.102558.

[4] Boldea I., "Linear electric machines, drives, and MAGLEVs handbook", CRC press (2017), doi: 10.1201/9781003227670.

[5] Hosseini M. S. and Vaez-Zadeh S., "Modeling and Analysis of Linear Synchronous Motors in High-Speed Maglev Vehicles," *IEEE Trans. Magnetics*, **46**(7), pp. 2656-2664 (2010), doi: 10.1109/TMAG.2009.2039999.

[6] Lorenzen H. W., Nuscheler R. and Meyer A., "Experimental investigation of the operating behaviour of linear synchronous motors," *IEEE Trans. Energy Convers.*, **EC-1**(4), pp. 73-82 (1986), doi: 10.1109/TEC.1986.4765778.

[7] Rahideh A., Ghaffari A., Barzegar A. and et al., "Analytical model of slotless brushless PM linear motors considering different magnetization patterns," *IEEE Trans. Energy Convers.*, **33**(4), pp. 1797-1804 (2018), doi: 10.1109/TEC.2018.2840712.

[8] Tootoonchian F. and Nasiri-Gheidari Z., “Cogging force mitigation techniques in a modular linear permanent magnet motor,” *IET Elect. Power Appl.*, **10(**7), pp. 667-674 (2016), doi: https://doi.org/10.1049/iet-epa.2015.0575.

[9] Huang X., Qian Z., Tan Q., et al., "Suppressing the thrust ripple of the permanent magnet linear synchronous motors With different pole structures by setting the modular primary structures differently," *IEEE Trans Energy Convers.*, **33(**4), pp. 1815-1824 (2018), doi: 10.1109/TEC.2018.2842077.

[10] Tan Q., Huang X., Li L. and et al., "Analysis of flux linkage and detent force for a modular tubular permanent magnet synchronous linear motor with large slots", *IEEE Trans. Energy Convers.*, **34(**3), pp. 1532-1541 (2019), doi: 10.1109/TEC.2019.2912873.

[11] Yoshida K., Lee J. and Kim Y. J., "3-D FEM field analysis in controlled-PM LSM for Maglev vehicle", *IEEE Trans. Magn.*, **33(**2), pp. 2207-2210 (1997), doi: 10.1109/20.582771.

[12] Andriollo M., Martinelli G., Morini A. and et al., "FEM calculation of the LSM propulsion force in EMS-MAGLEV trains," *IEEE Trans. Magn.*, **32**(5), pp. 5064-5066 (1996), doi: 10.1109/20.539491.

[13] Krämer C., Kugi A. and Kemmetmüller W., “Optimal force control of a permanent magnet linear synchronous motor with multiple shuttles”, *ISA Trans*, **140**, pp. 483-489 (2023), doi: 10.1016/j.isatra.2023.05.012.

[14] Krämer C., Kugi A. and Kemmetmüller W., “Optimal force control of a permanent magnet linear synchronous motor based on a magnetic equivalent circuit model”, *Control Eng Practice*, **122**, pp. 1-10, (2022), doi: 10.1016/j.conengprac.2022.105076.

[15] Jung I. S., Yoon S. B., Shim J. H. and et al., "Analysis of forces in a short primary type and a short secondary type permanent magnet linear synchronous motor," *IEEE Trans. Energy Convers.*, **14(**4), pp. 1265-1270 (1999), doi: 10.1109/60.815057.

[16] Lee D. Y., Jung C. G., Yoon K. J. and et al., "A study on the efficiency optimum design of a permanent magnet type linear synchronous motor," *IEEE Trans. Magn.*, **41**(5), pp. 1860-1863 (2005), doi: 10.1109/TMAG.2005.846466.

[17] Cho H., Sung H., Sung S. and et al., "Design and characteristic analysis on the short-stator linear synchronous motor for high-speed maglev propulsion," *IEEE Trans. Magn.*, **44(**11), pp. 4369-4372 (2008), doi: 10.1109/TMAG.2008.2001511.

[18] Zhi R., Liu B., Lv G., and et al., "Characteristics Analysis of Novel Transverse Flux Linear Synchronous Motor for Maglev Transportation," *IEEE Trans. Trans Electr*, **9**(3), (2023), doi: 10.1109/TTE.2023.3238744.

[19] Hwang C., Li P. and Liu C., "Optimal design of a permanent magnet linear synchronous motor with low cogging force", *IEEE Trans. Magn.*, **48(**2), pp. 1039-1042 (2012), doi: 10.1109/TMAG.2011.2172578.

[20] Dong F., Zhao J., Song J. and et al., "Optimal design of permanent magnet linear synchronous motors at multi-speed based on particle swarm optimization combined with SN ratio method," *IEEE Trans. Energy Convers.*, **33**(4), pp. 1943-1954 (2018), doi: 10.1109/TEC.2018.2841421.

[21] Lijuan Y., Shuyuan C., Jialong H. and et al., "Electromagnetic Design and Analysis of Permanent Magnet Linear Synchronous Motor", Energies, **15**(15), pp. 1-17 (2022), doi: 10.3390/en15155441.

[22] Heidary M., Naderi P., and Shiri A., "Modeling and analysis of a multi-segmented linear permanent-magnet synchronous machine using a parametric magnetic equivalent circuit", *Electr Eng*, **104**, pp. 705–715 (2022), doi: 10.1007/s00202-021-01334-1.

[23] Lv G., Zhang Z. and Li X., "Three-dimensional electromagnetic characteristics analysis of novel linear synchronous motor under lateral and yaw conditions of MAGLEV", *CES Trans on Elect Machines and Systems*, **6**(1), pp. 29-36 (2022), doi: 10.30941/CESTEMS.2022.00005.

[24] Rostami M., Naderi P. and Shiri A., "Modeling and detection of demagnetization fault in permanent magnet vernier machine using flexible magnetic equivalent circuit method", *Scientia Iranica*, **30**(4), pp. 1368-1381 (2023), doi: 10.24200/SCI.2021.59113.6067.

[25] Xu W., Xiao X., Du G. and et al., "Comprehensive efficiency optimization of linear induction motors for urban transit", *IEEE Trans. Vehic. Techn.*, **69(**10), pp. 131-139 (2020), doi: 10.1109/TVT.2019.2953956.

[26] Shiri A. and Shoulaie A., "Design optimization and analysis of single-sided linear induction motor, considering all phenomena", *IEEE Trans. Energy Convers.*, **27**(2), pp. 516-525 (2012), doi: 10.1109/TEC.2012.2190416.

[27] Shiri A. and Tessarolo A., "Normal force elimination in single-sided linear induction motor using design parameters", *IEEE Trans Trans Electr*, **9**(1), pp. 394-403 (2023), doi: 10.1109/TTE.2022.3183535.

[28] Fattahpour Roushan S. and Shiri A., "A new method for designing DC-excited linear synchronous motor", *11th Power Electr., Drive Sys., and Techno. Conf. (PEDSTC), Tehran, Iran* (2020), doi: 10.1109/PEDSTC49159.2020.9088488.

[29] Duncan J., "Linear induction motor-equivalent circuit model", *IEE Proc. Electr. Power Appl.*, **130**(1), pp. 51–57 (1983), doi: 10.1049/ip-b.1983.0008.

[30] Niknafs S., Shiri A. and Bagheri S., "Design and optimization of air-cored double-sided linear permanent magnet generators for wave energy conversion", *Energy Sci & Eng*., **10**(12), pp. 4481-4495 (2022), doi: 10.1002/ese3.1284.

[31] Valle Y., Venayagamoorthy G. K., Mohagheghi S. and et al., "Particle swarm optimization: basic concepts, variants and applications in power systems", *IEEE Trans. Evol. Comput.*, **12(**2), pp. 171-195 (2008), doi: 10.1109/TEVC.2007.896686.

Biographies

Soheil Fattahpour Roushan was born in Babol, Iran, in 1990. He received the B.Sc. degree in electrical engineering from Babol Noshirvani University of Technology, Babol, Iran in 2015, and the M.Sc. degree in electrical engineering from Shahid Rajaee Teacher Training University, Tehran, Iran, in 2020. His current research interests include linear electric machines and electrical machine design and modeling.

Abbas Shiri received the B.Sc. degree from Tabriz University and M.Sc. and Ph.D. degrees from Iran University of Science and Technology all in electrical engineering in 2004, 2006 and 2013, respectively. He is currently an associate professor at Shahid Rajaee Teacher Training University, Tehran, Iran. His areas of research interests include linear electric machines, electromagnetic systems and actuators, electrical machine design and modeling.

Peyman Naderi was born in Ahvaz, Iran, in 1975. He received his B.S. degree in Electronic Engineering in 1998 and M.S. degree in Power Engineering from Chamran University, Ahvaz, Iran in 2001. He has a Ph.D. degree in Power Engineering Science from K.N. Toosi University, Tehran, Iran. His interests are electrical machine modeling and fault diagnosis and also power system transient. He is currently associate professor in Shahid Rajaee Teacher Training University of Tehran, Iran.

Figure captions:

Table captions:

TABLE I: SPECIFICATION OF THE INVESTIGATED MOTOR

TABLE II: OPTIMIZATION RESULTS (SINGLE-OBJECTIVE)

TABLE III: OPTIMIZED VARIABLES IN MULTI-OBJECTIVE OPTIMIZATION

TABLE IV: OUTPUT RESULTS OF THE MULTIOBJECTIVE OPTIMIZATION

TABLE V: COMPARISON OF THE OUTPUTS AT DIFFERENT LOADS AT THE SAME LOAD-ANGLE

Figures:

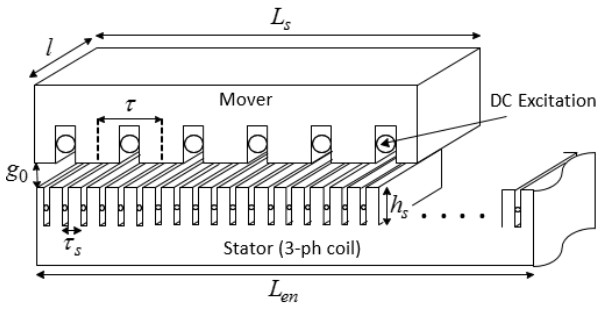

Fig. 1

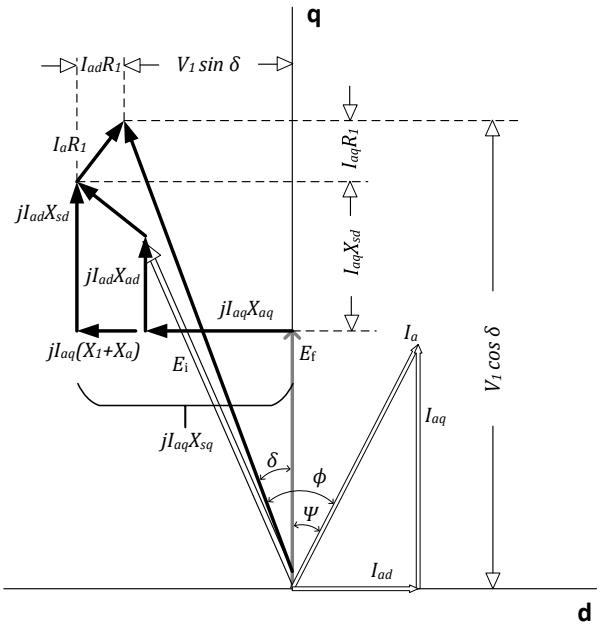

Fig. 2.

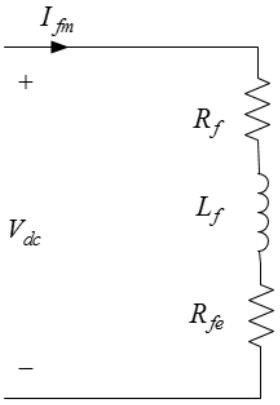
I_{fm}
+
R_f
L_f
V_{dc}
R_{fe}
−

Fig. 3

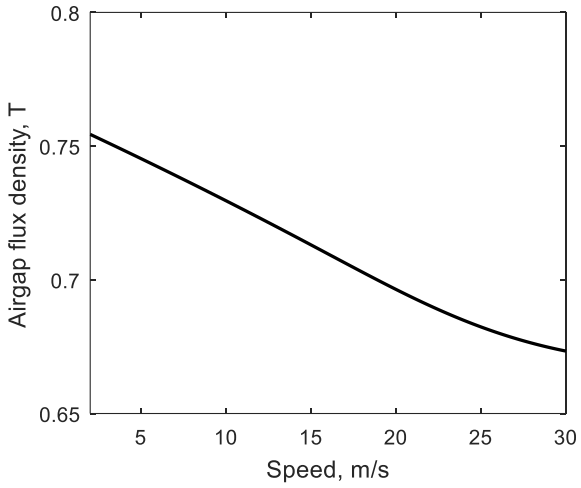
0.8
0.75
0.7
0.65
Airgap flux density, T
5
10
15
20
25
30
Speed, m/s

Fig. 4

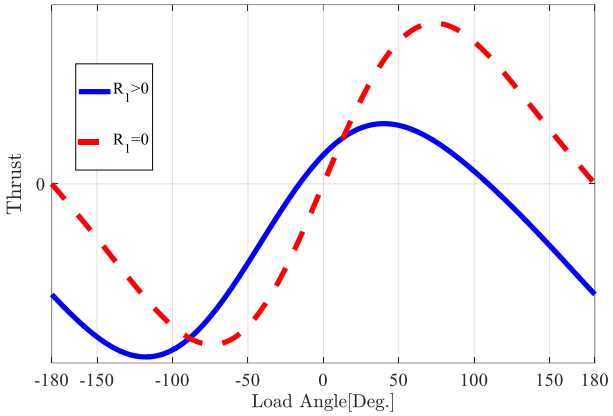
R1>0
R1=0
Thrust
0
-180 -150 -100 -50 0 50 100 150 180
Load Angle[Deg.]

Fig. 5

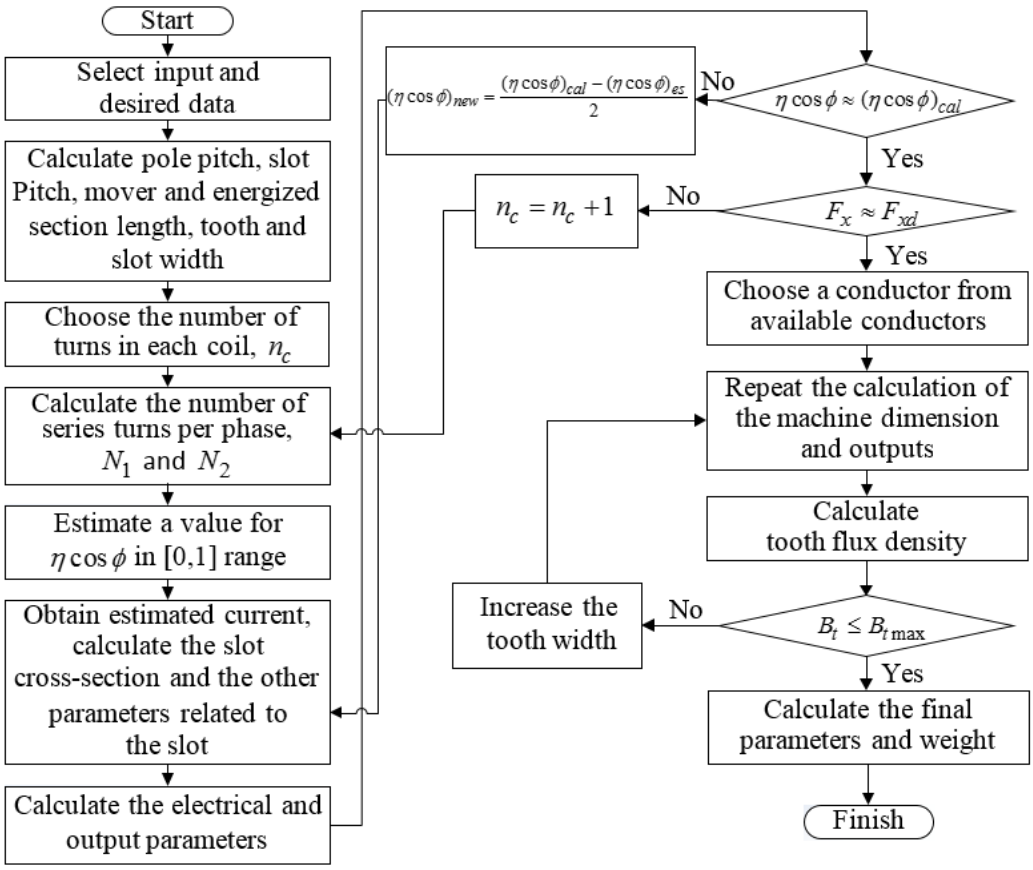
Start
Select input and desired data
Calculate pole pitch, slot Pitch, mover and energized section length, tooth and slot width
Choose the number of turns in each coil, n_c
Calculate the number of series turns per phase, N_1 and N_2
Estimate a value for $\eta\cos\phi$ in [0,1] range
Obtain estimated current, calculate the slot cross-section and the other parameters related to the slot
Calculate the electrical and output parameters
$(\eta\cos\phi)_{new} = \frac{(\eta\cos\phi)_{cal} - (\eta\cos\phi)_{es}}{2}$
No
$\eta\cos\phi \approx (\eta\cos\phi)_{cal}$
Yes
$n_c = n_c + 1$
No
$F_x \approx F_{xd}$
Yes
Choose a conductor from available conductors
Repeat the calculation of the machine dimension and outputs
Calculate tooth flux density
Increase the tooth width
No
$B_t \le B_{t\max}$
Yes
Calculate the final parameters and weight
Finish

Fig. 6

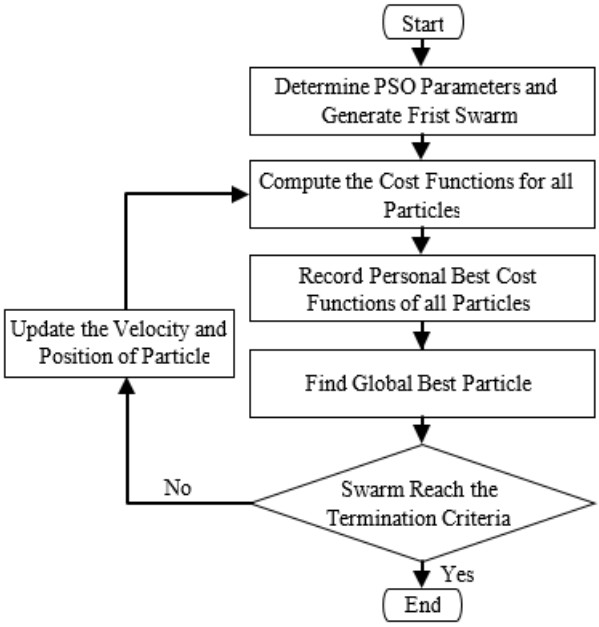
Start
Determine PSO Parameters and Generate Frist Swarm
Compute the Cost Functions for all Particles
Record Personal Best Cost Functions of all Particles
Find Global Best Particle
Swarm Reach the Termination Criteria
No
Yes
Update the Velocity and Position of Particle
End

Fig. 7

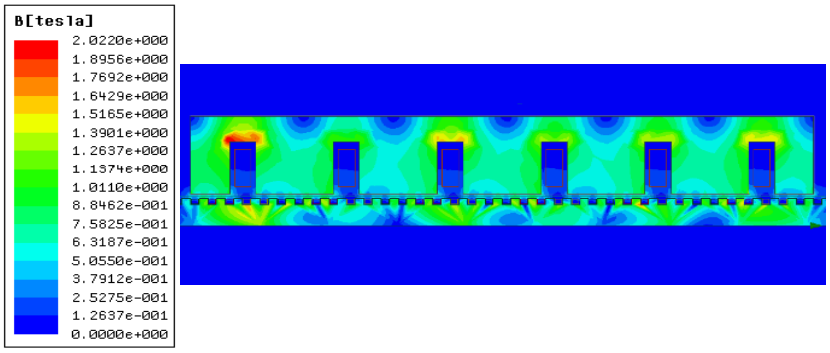
B[tesla]
2.0220e+000
1.8956e+000
1.7692e+000
1.6429e+000
1.5165e+000
1.3901e+000
1.2637e+000
1.1374e+000
1.0110e+000
8.8462e-001
7.5825e-001
6.3187e-001
5.0550e-001
3.7912e-001
2.5275e-001
1.2637e-001
0.0000e+000

Fig. 8

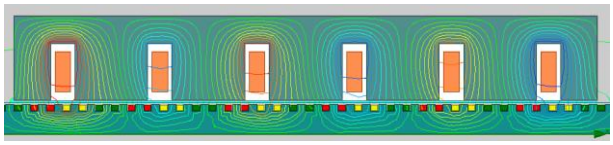

Fig. 9

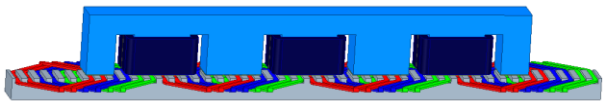

Fig. 10

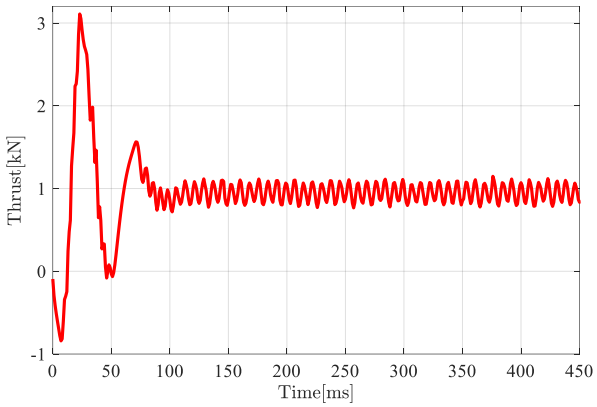

Fig. 11

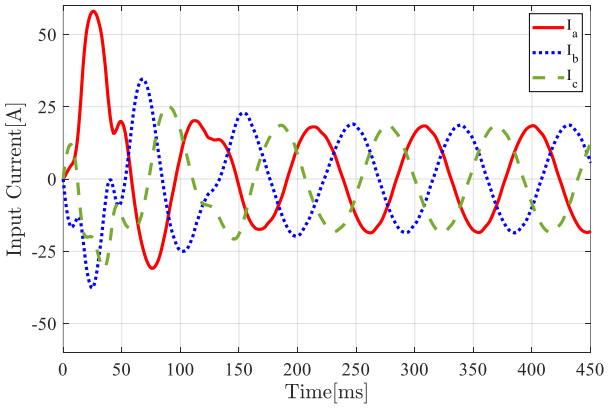

Fig. 12

Tables:

TABLE I

Parameter	Value
Phase input voltage [V]	220
Stator input frequency [Hz]	10.8
Pole pairs, (p)	3
Slots/pole/phase, (q)	2
Tooth width [mm]	19.29
Machine width [mm]	90
Air-gap length [mm]	10.6
Load-angle [Deg.]	12.75
Stator current density [A/mm^2]	3
Secondary magnetomotive force [A-T]	8788.4

TABLE II

Parameter	Range		Optimized values			
	Min	Max	Power factor optimization	Efficiency optimization	Rail weight/Length optimization	Mover weight optimization
Input frequency, Hz	10	100	15.4	10.7	100	17
Machine width, mm	20	200	200	200	87	20
Air-gap length, mm	10	30	30	10	10.3	10
Tooth width/Slot pitch	0.3	0.5	0.5	0.5	0.5	0.35
Number of slots/pole/phase	1	2	1	2	2	2
Load-angle, Deg.	0	90	59.7	10.14	90	22.8
Objective function	-		1	76 %	61.135 kg/m	71.219 kg

TABLE III

Parameter	Range		Optimized Values
	Min	Max	
Input frequency [Hz]	10	100	10.8
Machine width [mm]	20	200	90
Air-gap length [mm]	10	30	10.6
Tooth width/slot pitch	0.3	0.5	0.5
Number of slots/pole/phase	1	2	2
Load-angle [Deg.]	0	90	12.75

TABLE IV

Outputs	Optimized values
Thrust [N]	953.42
Input Current [A]	12.61
Induced Voltage [V]	153.02
Power Factor	0.9038
Efficiency [%]	63.36
Rail weight/Length [kg/m]	86.96
Mover weight [kg]	480.64

TABLE V

	Quantity	Proposed Method	2-D FEM	3-D FEM
Load 1 (Full-load) (953.42 N)	Input Current [A]	12.61	13.14	13.02
	Induced Voltage [V]	153.02	148.98	151.52
	Power Factor	0.904	0.878	0.905
	Efficiency [%]	63.36	62.61	61.30
Load 2 (475 N)	Input Current [A]	9.63	10.04	9.93
	Induced Voltage [V]	165.32	161.21	162.84
	Power Factor	0.649	0.631	0.658
	Efficiency [%]	57.58	56.80	55.07